X International Conference on Computational Methods in Marine Engineering
MARINE 2023
J. García-Espinosa, L. González, J.E. Gutiérrez & B. Serván-Camas (Eds)

Shape Optimization of a Naval Destroyer by Multi-Fidelity Methods

A. Serani[1*] , S. Ficini[1], R. Broglia[1], M. Diez[1], O. Goren[2], D. B. Danisman[2], H. Pehlivan Solak[2], S. Yıldız[2], M. Nikbay[2], T. Scholcz[3], J. Klinkenberg[3], G. Grigoropoulos[4], C. Bakirtzoglou[4], and G. Papadakis[4]

[1]National Research Council-Institute of Marine Engineering (CNR-INM), Rome, Italy
[2]Istanbul Technical University (ITU), Istanbul, Turkey
[3]Maritime Research Institute Netherlands (MARIN), Wageningen, The Netherland
[4]National Technical University of Athens (NTUA), Athens, Greece
[*] Corresponding author: andrea.serani@cnr.it

ABSTRACT

The paper presents and discusses the shape optimization of a destroyer-type vessel by means of several multi-fidelity approaches. The hull-form design (bare hull) of the DTMB 5415 model (an open-to-public concept used in the development of the DDG-51, the lead vessel of the Arleigh Burke-class guided missile destroyers) is addressed for optimal resistance performance in calm water and formulated as a global optimization problem. The design performance is assessed using a variety of physical models and solvers (from potential flow models to Reynolds-Averaged Navier Stokes equations), and spatial discretizations, which are combined together in dedicated multi-fidelity frameworks developed within the activities of the NATO-AVT-331 Research Task Group on "Goal-driven, multi-fidelity approaches for military vehicle system-level design." Problems description, design parameterization methods, physical models and solvers are presented and discussed, as well as multi-fidelity approaches and results. The present effort highlights how the dimensionality of the optimization problem may be a critical issue for the surrogate model training. Nevertheless, it is shown how the proposed multi-fidelity approaches are able to achieve significant design performance improvements, even if only a few high-fidelity computations are used, with a ratio between the number of high- and low-fidelity evaluations required to solve the global optimization problem as low as nearly 1/50. Finally, the challenges arisen during the process are discussed and future research directions outlined.

Keywords: Shape optimization; Multi-fidelity methods; Computational fluid dynamics; DTMB 5415.

1. INTRODUCTION

The design process of novel vessels is experiencing a methodological revolution, due to the development of ever-fast and powerful high-performance computing (HPC) systems and efficient simulation-driven design optimization (SDDO) frameworks. Generally, the accuracy of SDDO solutions requires high-fidelity and therefore computationally expensive computer simulations, such as high-fidelity computational fluid dynamics (CFD). For example, a statistically significant CFD-based evaluation of ship performance in irregular seaways may require up to 1M CPU hours on HPC systems (Serani et al., 2021). The computational cost required to evaluate design objectives and constraints further increases if multi-disciplinary/multi-physics, multi-point, and multi-objective problems need to be addressed, such as in the hydro-structural optimization of vessels at multiple speeds and conditions (Serani et al.,

2022b). Consequently and despite the availability of powerful HPC systems, the extensive use of high-fidelity simulation tools can be impractical in ship design optimization, especially when high-dimensional design spaces are explored for global optima.

Multi-fidelity (MF) approaches have shown their potential to alleviate the computational cost associated with the solution of high-fidelity SDDO problems, by combining multiple information sources, such as multiple physical models and solvers, space/time discretizations, and levels of physical coupling. Nevertheless, the full potential and application domain of MF methods are still the subject of discussion in the SDDO community, as MF methods feature a great number of different approaches, settings, and applications. Within this context, the NATO Applied Vehicle Technology (AVT), Research Task Group 331 on "Goal-driven, multi-fidelity approaches for military vehicle system-level design" has rigorously addressed the capability of MF methods to solve design optimization for military vehicles in an efficient and effective way. To this aim, the Task Group proposed the use of three types of benchmark problems for the assessment of MF methods, characterized by different levels of complexity, namely L1 (analytic problems), L2 (simple problems of engineering/vehicle relevance), and L3 (Beran et al., 2020). L3 problems use partial differential equations solutions, exhibit physical coupling of two or more disciplines/systems, are affected by moderate to large numerical errors/uncertainties, have a high computational cost, and address vehicle-level engineering models.

The objective of the present work is to present and discuss the effort in solving the most complex type of problems, namely the L3 sea benchmark problems, within the activities of the AVT-331 (Serani et al., 2022a). These pertain to the hull-form optimization of a destroyer-type vessel for reduced resistance performance. The DTMB 5415 model is used as a parent design, which is an open-to-public concept used in the development of the DDG-51, the lead vessel of the Arleigh Burke-class guided-missile destroyers. The DTMB 5415 has been widely used in the community for computational and experimental studies, as well as in earlier AVT efforts. Different combinations of problem formulations, design space parameterizations, physical models and numerical solvers, and finally MF approaches are investigated here. Specifically five MF optimization frameworks are developed and tested and are here presented and discussed. Hull-form parameterizations include free-form deformation (FFD, Sederberg and Parry 1986), Akima's surface generation (Akima, 1978), hull blending, and computer-aided design (CAD) parametric modeling approaches. Different governing equations (RANS and

Figure 1: Starboard bow view of the guided missile destroyer Arleigh Burke (DDG-51, left) and corresponding digital counterpart of the DTMB 5415 model (right).

potential flow) and solvers, with different computational grid sizes, are considered for the MF solution of the design problem. Finally, MF integration methods are mainly based on surrogate models, such as multi-fidelity/source/level radial basis functions, Gaussian process/Kriging, as well as Artificial Neural Networks (ANN).

The focus of the paper is on discussing the ability of MF approaches to achieve high-fidelity globally optimal design decisions with only a few high-fidelity evaluations, therefore saving computational time and cost. It is worth noting that, although a direct comparison of MF framework capabilities and results is of certain interest, when dealing with L3 type of problems (at least for the present case) this encounters a number of barriers, spanning from CAD (computer-aided design) and CFD tools availability and licenses associated to proprietary software, to heterogeneous availability of CPU hours and men power across Team Members. For these reasons, the present benchmark problem is dedicated to demonstrating MF methods' capabilities for complex industrial problems, albeit with limited comparison.

2. PROBLEM STATEMENT

The problem consists of the hull-form design of the DTMB 5415 model (see Fig. 1). This has been widely used for towing tank experiments (Olivieri et al., 2001), CFD studies (Sadat-Hosseini et al., 2015), and hull-form optimization (Serani et al., 2016a). The model main particulars (bare hull) are summarized in Tab. 1, where the length parameter $L_{\rm pp}$ is calculated from the forward perpendicular to the transom bottom edge.

The optimization problem considers a single-point calm-water condition. Specifically, the problem pertains to the single-objective constraint minimization of the total resistance ($R_{\rm T}$) in calm water at Froude number (Fr) equal to 0.28 (corresponding to 20kn at full scale) and reads

$$\begin{aligned} \text{minimize} \quad & R_{\rm T}(\mathbf{x}) \\ \text{subject to} \quad & L_{\rm pp} = L_{\rm pp_0} \\ \text{and to} \quad & \nabla(\mathbf{x}) \geq \nabla_0 \\ & |B(\mathbf{x})/B_0 - 1| \leq 0.05 \\ & |T(\mathbf{x})/T_0 - 1| \leq 0.05 \\ & V_d(\mathbf{x}) \geq V_0 \\ & \mathbf{x}_l \leq \mathbf{x} \leq \mathbf{x}_u \end{aligned} \tag{1}$$

where $\mathbf{x} \in \mathbb{R}^N$ is the design variable vector (related to shape parameterization), with $\mathbf{x}_l$ and $\mathbf{x}_u$ its lower and upper bounds. The problem uses an equality constraint for the length between perpendiculars $L_{\rm pp}$, whereas inequality constraints are given for displacement (∇), beam (B), draft (T), and the volume

Table 1: DTMB 5415 main particulars

Description	Symbol	Unit	Full scale	Model scale
Displacement	∇	tonnes	8,437	0.549
Length between perpendiculars	$L_{\rm pp}$	m	142.0	5.720
Beam	B	m	18.90	0.760
Draft	T	m	6.160	0.248
Longitudinal center of gravity	LCG	m	71.60	2.884
Vertical center of gravity	VCG	m	1.390*	0.056*

* Above the water line

reserved for the sonar in the bow dome (V_d), where subscript '0' refers to the parent hull values. Specifically, the displacement has to be greater or equal to the parent hull, whereas $\pm 5\%$ variation of beam and draft is allowed (Grigoropoulos et al., 2017). The physical coupling of hydrodynamics with rigid-body equations of motion is also considered.

Three sub-problems have been defined:

1. total resistance minimization at model scale, including coupling with the rigid-body equation of motions (trim and sinkage are free and the dynamic equilibrium has to be found)
2. total resistance minimization at model scale at even keel (trim and sinkage are inhibit)
3. total resistance minimization at full scale, including coupling with the rigid-body equation of motions

3. MULTI-FIDELITY OPTIMIZATION FRAMEWORKS

Hull-form parameterization approaches, physical models/solvers, and MF integration methods are combined to form five MF optimization frameworks, each investigated by a single institution participating in the AVT-331 Sea Team, as described in the following subsection and summarized in Tab. 2.

3.1 Framework A

FFD is used to generate design variants and modify the associated computational grid. The number and coordinates of control points (CPs) are chosen to generate both local and global modifications of the hull, based on earlier experience within AVT-204 Grigoropoulos et al. (2017). Specifically, the design space is formed by $M = 22$ design variables; the demi-hull is put in a lattice of $9 \times 3 \times 3$ nodes in the $\xi_1\xi_2\xi_3$ reference system; only 21 nodes are active (see the blue sphere in Fig. 2), all with only one degree of freedom (DoF), except for one that has 2 DoF; the shape modification is achieved by interpolating the CPs' modification over the embedding space, using a tensor product of trivariate Bernstein polynomials. A detailed description of DoF and associated design variables can be found in Serani and Diez (2023). In order to deal with the curse of dimensionality problem, the design space is reduced in dimensionality using parametric model embedding (PME, Serani and Diez 2023). The method is simulation-free and uses a generalized feature space that included shape modification and design variables vectors with a generalized inner product. This allows to reduce the dimensionality of the design space, retaining at least a prescribed level of geometrical variance of the original design space. The method is fed by a bunch of hull variants and the associated design parameters and provides a reduced-order model of the original design parameterization, allowing its direct reconstruction.

Table 2: Multi-fidelity optimization frameworks

Frameworks	Problems	Design parameterization	Solvers	MF approaches	Team
A	1	FFD/PME	CFDShip-Iowa, WARP	SRBF	CNR-INM
B	1	Akima	OpenFOAM, ITU-Dawson	KPLS	ITU
C	1	Blending	ReFRESCO	KG-AEI	MARIN
D	2	FFD	χnavis	SRBF	CNR-INM
E	3	Parametric CAD	MaPFlow, SWAN2	Mixed-ANN	NTUA

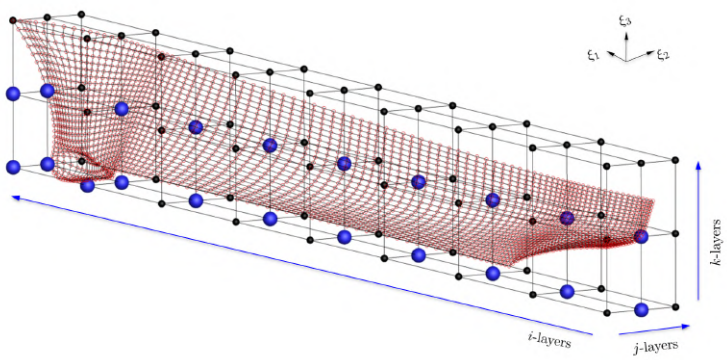

Figure 2: FFD parameterization (framework A and D)

The MF approach uses a stochastic radial basis function (SRBF) surrogate model with active learning, based on the lower confidence bounding method (Serani et al., 2019; Pellegrini et al., 2022; Wackers et al., 2022), and leverage on RANS and potential flow simulations. Specifically, the high-fidelity is based on the CFDShip-Iowa V4.5 code (Huang et al., 2008) an incompressible URANS solver designed for ship hydrodynamics and developed at the University of Iowa. It models the free surface with a single-phase capturing approach, meaning that only the water flow is solved, enforcing kinematic and dynamic free-surface boundary conditions on the interfaces. It uses structured multiblock grids and has overset capabilities. In the present study, the URANS equations are solved in the ship coordinate system. The turbulence is computed by the isotropic Menter's blended $k-\omega/k-\epsilon$ model with shear stress transport. A second-order upwind scheme is used to discretize the convective terms of momentum equations. A projection method for pressure/velocity coupling is used. The low-fidelity is based on the WARP code, a linear potential flow solver developed at CNR-INM (Bassanini et al., 1994). Wave resistance computations are based on the Dawson (double-model) linearization (Dawson, 1977), whereas the frictional resistance is estimated using a flat-plate approximation, based on the local Reynolds number (Schlichting and Gersten, 2000). The resistance is evaluated by the integration of pressure and friction over the body surface. The steady 2DoF (sinkage and trim) equilibrium is achieved by iteration of the flow solver and the body equation of motion.

Finally, surrogate model active learning and the optimization problem 1 are solved via a memetic single-objective deterministic particle swarm optimization algorithm (DPSO, Serani et al. 2015), whose setup is based on Serani et al. (2016b).

3.2 Framework B

Akima's surface generation method, from a set of scattered points (see Fig. 3), is used to define the hull surface related to the coefficients associated to some control points. To have a finer mesh, the relaxation coefficients for other intermediate (interpolation) points are obtained by interpolation using the relaxation coefficients defined at the control points. Since there is no precisely defined fairness criterion in the present work, no fairing on the wetted surface of the hull is applied. Note that the relaxation coefficient value is kept between 0.9 and 1.1 which is also subjected to the beam allowance limited to $\pm 5\%$ change only. Ultimately, the hull generation code creates new sections by interpolating the modified waterlines to prepare input data for the wave resistance code explained in the following.

The MF approach is used to solve problem 1 and is based on Kriging Partial Least Squares (KPLS),

Figure 3: Akima's surface parameterization (framework B)

which is a modified version of Kriging derived by Bouhlel et al. (2016) that uses the PLS approach and reduces the number of hyperparameters to be optimized while maintaining a successful estimation accuracy. The PLS coefficients are calculated using linear dependence between input and outputs and this relation is used in the modified correlation function of inputs for deriving the KPLS method. MF data comes from RANS and potential flow computations. Specifically, HF samples are based on the open-source RANS solver OpenFOAM. It employs an earth and body fixed Cartesian coordinate system, with z-axis upward positive and the ship is free to sink and trim. The volume of fluid (VoF) approach is used to model the two flow phases of water and air above the still water level. The $k-\omega$ SST turbulence model is employed in order to solve the turbulence equations. A first-order implicit (Euler) scheme is applied to discretize the unsteady term in Navier-Stokes equations. PIMPLE algorithm, a combination of PISO and SIMPLE (Semi Implicit Methods Pressure Linked Equations) algorithms, is used to solve the pressure-velocity coupling. Low-fidelity computations are based on ITU-Dawson, an ITU in-house code, which utilizes the usual assumptions for the non-lifting potential flow: wave resistance analyses are carried out by ITU-Dawson and total resistance is determined by adding viscous resistance obtained from ITTC-1957 friction line accompanied with a computed form factor. It calculates the unknown velocity potential by using a source/sink distribution over the panels, according to Hess and Smith's method, distributed on the wetted surface of the ship as well as on a portion of the free surface in the vicinity of the hull. The free-surface condition is linearized according to the low-Froude number theory and is satisfied by means of a numerical scheme introduced by Dawson (1977). A wet transom boundary condition is imposed (Maisonneuve, 1989). Actual (dynamic) sinkage and trim are applied to the hull by an iterative procedure.

Finally, the optimization process is performed by using SciPy's differential evaluation tool (Storn and Price, 1997) which is a widely used stochastic population-based method for global optimization problems.

3.3 Framework C

A hull-blending technique is used to parameterize the hull shape. A small number of basis hull designs are chosen which define the scope of the deformations. Let H_0 denote the "original" hull shape. The other basis shapes are then denoted by H_i with $i = 1, \ldots, N$, each characterizing a type of deformation. Each basis shape is defined by N_c control points of a B-spline surface. The parameterized control points are then obtained by linear interpolation on the control points of the basis designs, with coefficients representing the contribution of a certain shape deformation of the corresponding basis shape in the "hull-blend". The basis shapes used here are shown in Fig. 4.

The MF approach uses a multi-fidelity Kriging method (Huang et al., 2006), with active learning based on an augmented expected improvement (AEI, Scholcz and Klinkenberg 2022), and leverage on RANS simulations with different grid discretization. Specifically, RANS computations are based on the ReFRESCO code. It is an unstructured-grid free-surface capturing method that solves the steady wave pattern problem by time integration. It is based on the finite volume formulation and can work with all types of cells, making it compatible with a wide variety of grid generation packages. Adaptive

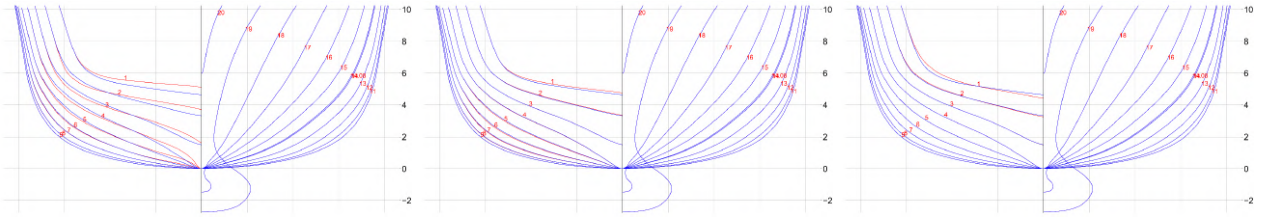

(a) H_1: Aft buttocks S-shape (b) H_2: Transom immersion (c) H_3: V-shape

Figure 4: Blending Parameterization Basis Hull Shapes (framework C)

grid refinement capabilities help further with focusing the cells and computational resources at crucial locations. Various turbulence models, from RANS models to high-fidelity hybrid and scale resolving models, complemented with transition models are available to answer the most common maritime engineering challenges.

Finally, surrogate model active learning and optimization problem 1 are solved using a restarted L-BFGS-B method (Byrd et al., 1995).

3.4 Framework D

Framework D is used to solve problem 2, combining FFD design space with the SRBF method, as in framework A, but the MF approach is trained by only a RANS solver, leveraging on different grid discretization. Specifically, RANS computations are based on χnavis, an in-house code, developed at the CNR-INM (Di Mascio et al., 2001, 2009; Posa and Broglia, 2019). χnavis is based on a finite-volume discretization of the URANS equations, in which the flow variables are collocated at center-cells. Turbulent stresses are related to the gradients of velocity via the Boussinesq hypothesis. The turbulence viscosity is computed using the Spalart and Allmaras (1992) turbulence model. No wall functions are used, so the first grid elements on the wall ensure the $y^+ = 1$ condition. Free-surface effects are modeled using a single-phase level-set approach (Di Mascio et al., 2007; Broglia and Durante, 2018). To treat complex geometries or bodies in relative motion, the numerical algorithm is discretized on a block-structured grid with partial overlap, possibly in relative motion. The solver uses a full multi-grid full approximation scheme (FMG–FAS), with an arbitrary number of grid levels. In the FMG–FAS approximation procedure, the solution is computed on the coarsest grid level first. Then, it is approximated on the next finer grid and the solution is iterated by exploiting all the coarser grid levels available with a V-Cycle. The process is repeated up to the finest grid level. Thus, the procedure provides multi-fidelity data without any additional computational cost.

3.5 Framework E

The CAESES software is used for the parametric design and variation of the parent hull. The initial geometry is represented by a set of basic curves providing topological information in the longitudinal direction (design waterline, centerline, deck-line) and a set of 19-section curves. All of them are either F-splines or B-splines. The geometry is split into three regions: the main hull, the sonar dome, and the skeg, assigning specific design variables for each of them. The main hull part was split into five lofted surfaces, involving a skeg surface too. The separation of the hull to the main and fore parts is related to the selected way of approximating the initial surfaces and to the fact that the design variables for the main hull form concerned only its fore part. Thus, the fore part of the hull form was split into six parts, and five design variables of the lower dome's surface were employed. A total

Table 3: Parametric CAD model (framework E)

x_i	Description	Lower bound [m]	Upper bound [m]
1	Maximum Beam at Station 0	6.5	7.2
2	Maximum beam of sonar dome	2.9	3.6
3	Angle of Entrance	185.3	195.3
4	Wedge Depth	0.0	0.6
5	Maximum Beam at WL	9.0	9.8
6	Aft longitudinal position of sonar dome's lower profile	125.8	126.5
7	Forward longitudinal position of sonar dome's lower profile	140.8	142.5
8	Height of Skeg	1.5	2.5
9	Longitudinal position of sonar dome's maximum beam	135.8	138.0
10	Sonar dome's tip elevation (for the most forward point of sonar dome's length)	-1.7	-1.3

number of $N = 10$ design variables is employed, five of which are used to define the sonar dome. The range of variation has been selected to lead to realistic hull forms and smooth lines. In addition, upper and lower boundaries comply with the geometrical constraints as defined. Table 3 provides the range of the design variables and their values for the parent hull form.

The MF approach combines an ANN optimization methodology for the minimization of governing viscous resistance at the stern region while employing a separate optimization scheme for the bow and middle region of the hull by using a potential flow solver, together accounting for the objective of total calm-water resistance of problem 3. High-fidelity viscous computations are based on the MaPFlow code. It is an NTUA in-house URANS cell-centered solver, that can use both structured and unstructured grids, capable of solving compressible flows, as well as fully incompressible flows using the artificial compressibility method. For the reconstruction of the flow field, a 2nd order piecewise linear interpolation scheme is used. The limiter of Venkatakrishnan (1993) is utilized when needed. The viscous fluxes are discretized using a central 2nd-order scheme. Turbulence closures implemented on MaPFlow include the one-equation turbulence model of Spalart and Allmaras (1992) as well as the two-equation turbulence model of Menter ($k-\omega$ SST, Menter 1994). Regarding laminar to turbulent transition modeling, the correlation $\gamma - \mathrm{Re}\theta$ model of Langtry and Menter (2009) has been implemented. Time integration is achieved in an implicit manner permitting large CFL numbers. The unsteady calculations use a 2nd order time accurate scheme combined with the dual time-stepping technique to facilitate convergence. MaPFlow can handle moving/deforming geometries through the arbitrary Eulerian-Lagrangian formulation. The free surface is treated via the VoF method, where two-phase flows are described by two immiscible fluids with their interface being defined implicitly as a discontinuity in the density field. The system of equations is solved in a non-segregated manner, utilizing the Kunz Preconditioner, as discussed by Yue and Wu (2018), to remove density dependencies from the system's eigenvalues. Low-fidelity computations are based on the SWAM2 software package, developed at MIT. It distributes quadrilateral panels over the ship hull and the free surface to derive numerically the steady and unsteady free-surface potential flow around ships, using a three-dimensional Rankine Panel Method in the time domain. A batch file is used to integrate SWAN2 with the CAESES.

Finally, the mixed-fidelity approach uses a combination of low-fidelity computational solutions with ANN prediction of high-fidelity information. ANNs are used to model or detect complex nonlinear relationships within systems without using the physics of the system. They are composed of internal parameters to be specified through the process of training. Such parameters are the weights by which the inputs of each neuron are multiplied so that the corresponding output emerges. These weights are tuned so that the error of the output of the ANN (the last layer of neurons) over the available actual data is minimized. The development of the ANN was performed in Python assisted by the

Tensorflow/Keras neural network library.

4. RESULTS

The results obtained using the MF frameworks summarized in Table 2 and presented in the previous section are provided and discussed in the following subsections.

4.1 Framework A

URANS (CFDShip-Iowa) computational domain is composed of a background (3.5M points) and a boundary layer (∼1M points) volume grids, taking advantage of problem symmetry. The boundary layer volume grid is designed to have $y^+ < 1$, avoiding the use of wall functions. A detail of the computational grid is shown in Fig. 5 (left). The potential flow (WARP) computational domain is composed of the free-surface (7.6k points) and the hull (9k points) surface grids, taking advantage of problem symmetry. A detail of the computational grid is shown in Fig. 5 (right).

A comparison of HF and LF pressure fields and wave elevation patterns for the original hull is shown in Fig. 6. Pressure distributions are in reasonable agreement, whereas the wave elevation obtained by potential flow presents under-predicted diverging bow waves and over-predicted diverging stern waves.

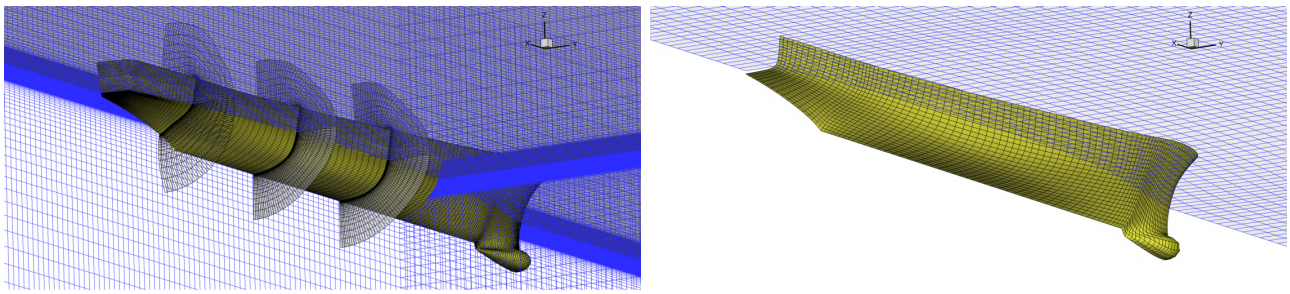

Figure 5: Computational grids for HF (left) and LF (right) solvers (framework A)

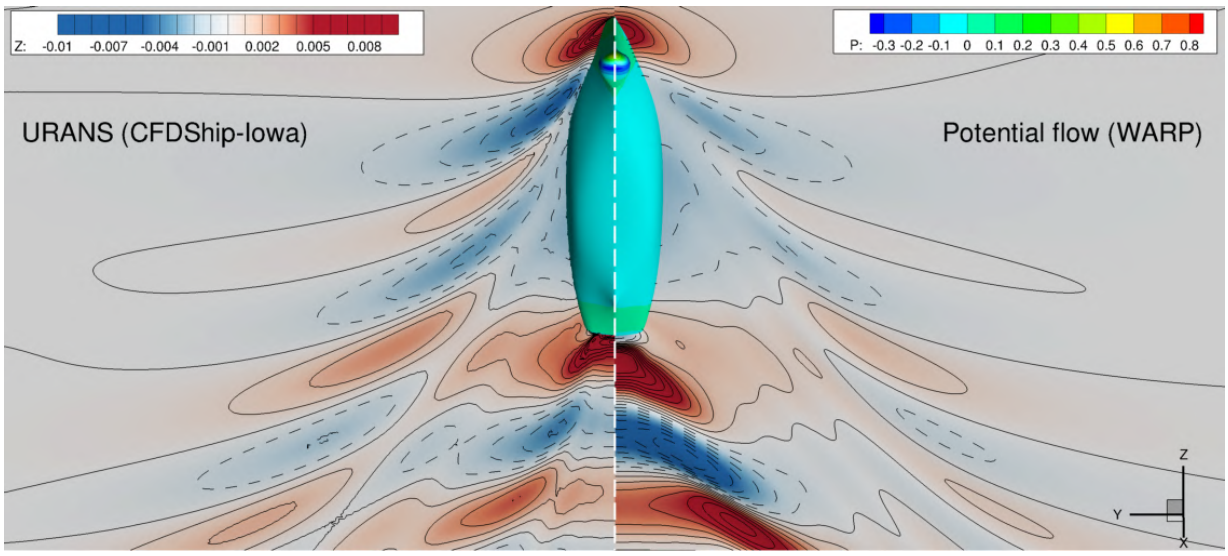

Figure 6: Comparison of URANS (left) and PF (right) wave elevation pattern and pressure field along the original hull (framework A)

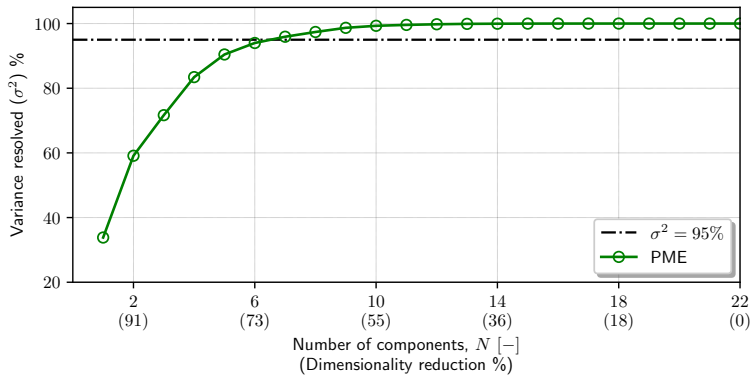

Figure 7: Design-space dimensionality reduction results via PME (framework A)

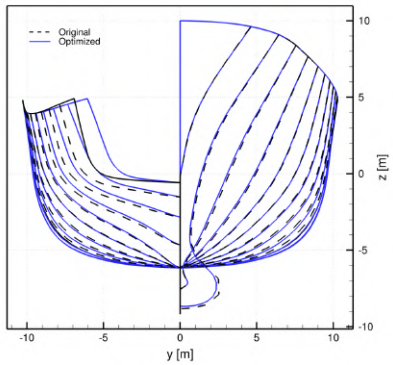

Figure 8: Comparison of original and the optimized hull stations (framework A)

The computation cost ratio between HF and LF solvers is equal to 0.001.

Since surrogate models suffer from the curse of dimensionality, their training can be quite expensive with high-dimensionality problems. Therefore, the original FFD ($M = 22$ design parameters) is reduced in dimensionality through PME (Serani and Diez, 2023). Specifically, PME is trained by 1000 Monte Carlo realizations of the design space (each realization is a modified hull shape and the associated design parameters) achieving a dimensionality reduction of almost 70% ($N = 7$), retaining at least the 95% of the original geometrical variance. The cumulative sum of the variance resolved as a function of the PME-reduced design variables is shown in Fig. 7. MF surrogate model begins with an initial training set composed of a face-centered central composite design (CCF) for the LF level, corresponding to 15 training points, and only 1 HF training point in the domain center. Optimization is stopped when 15 high-fidelity samples are added to the training set. The optimum is achieved by training the SRBF method with 15 HF and 647 LF evaluations, providing 5.8% resistance reduction. A comparison with the original hull stations is shown in Fig. 8. Specifically, it can be seen how the optimum has basically not changed the forward part of the vessel, whereas a significant restriction of the stern region is achieved. This latter result affects both pressure and wave elevation fields as shown in Fig. 6. Specifically, the optimized hull provides a better recovery of the pressure towards the stern, as well as a mild reduction of the diverging stern waves.

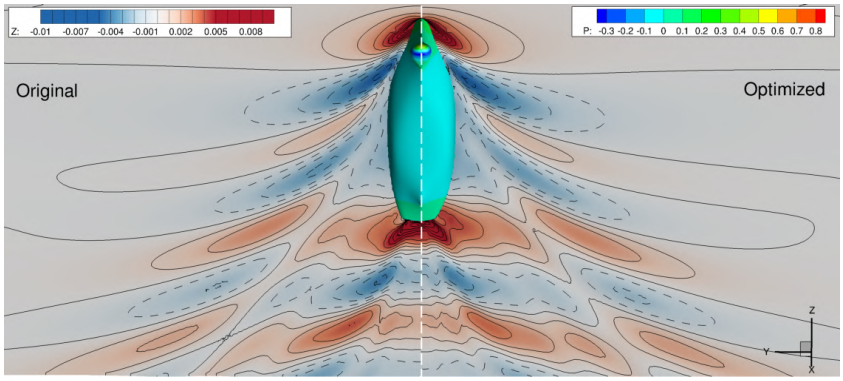

Figure 9: Comparison of original and the optimized wave elevation pattern and pressure field along the hull (framework A)

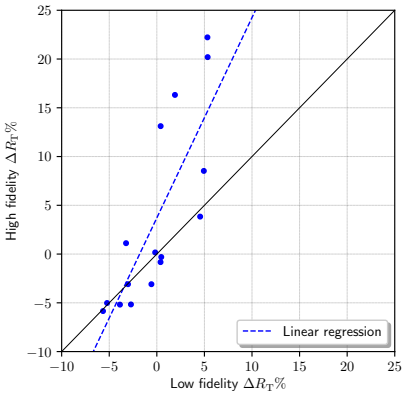

Figure 10: Objective functions correlation for HF and LF numerical solutions (framework A)

One last analysis of the MF-based optimization outcomes has been conducted on the correlation of the information sources. Specifically, Fig. 10 provides the objective functions relative variation of the LF vs HF training points. A quite good correlation between the two information sources is shown by the linear regression line (blue dashed), even if not perfect (represented by the continuous black line), meaning that, for this specific problem, the potential flow can be quite effective (probably when no separation phenomena occurs), but at the same time can provide huge under/overestimation of the objective function variation, probably due to separation phenomena, that cannot be modeled.

4.2 Framework B

RANS (OpenFOAM) computational domain and boundary conditions are determined by following the ITTC guidelines: inlet, bottom, and side boundaries are fixed as $2L_{\text{pp}}$ from the ship model, and the outlet boundary is placed $3L_{\text{pp}}$ downstream direction in order to minimize the effect of wave reflection from boundaries of the numerical domain; lateral sides and bottom boundaries were assigned as symmetry plane, inlet, outlet, and atmosphere boundary conditions are determined associated with the turbulence parameters and flow characteristics, and, finally, the wall-type boundary condition is adopted for hull surface. Mesh generation is adopted by using the BlockMesh utility in OpenFOAM. In order to refine the mesh so as to be close to the hull surface, the TopoSet utility is applied for enhancing the mesh density. Two control volumes are modeled around the hull form to resolve the flow characteristics, then snappyHexMesh is implemented to conclude the 3D mesh generation process. A total of $\sim 2M$ grid points are used as the HF model (see Fig. 11 left). For potential flow (ITU-Dawson) solutions, which are employed for LF data, 1.8k panels over the hull surface (demi-hull) and 2k panels over the free surface (half symmetric plane) are used.

To deeply and systematically investigate the performance of the KPLS method: i) the number of PLS components are taken as 3 (KPLS3) and 4 (KPLS4) and ii) the number of the data associated with different fidelities are selected as diverse combinations. A Design of Experiments (DoE) of 1000 LF samples is used. To assess the prediction performance of the surrogate model, two global accuracy metrics are used: coefficient of determination (R^2) and root-mean-square error (RMSE). Surrogate model performance assessments are presented in Table 4, where 30 HF test data are used to determine the error metrics. Global error metrics are presented as their normalized values. Normally, it is expected that, as the number of data increases in one or in both of the fidelities, the R^2 should be increased, ideally reaches to 1 which means the surrogate model produces accurate/exact predictions, and RMSE decreases. Nevertheless, this is not the case. One may deduce for some specific combinations the MF surrogate modeling results in high correlation and highly reduced RMSEs, although it may be misleading to derive solid conclusions; furthermore, a relatively higher number of HF data

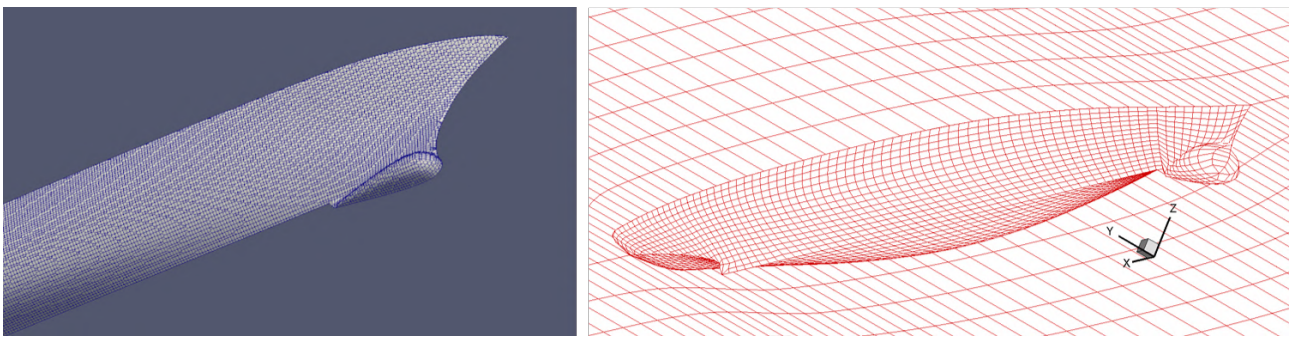

Figure 11: Computational grids for HF (left) and LF (right) solvers (framework B)

Table 4: KLPS performance with framework B

Train. set size		KPLS3						KPLS4					
LF	HF	$R^{2\star}$	RMSE*	$\hat{f}^*$ [N]	f^{**} [N]	$\Delta\%E^\dagger$	$\Delta\%R^\ddagger$	$R^{2\star}$	RMSE*	$\hat{f}^*$ [N]	f^{**} [N]	$\Delta\%E^\dagger$	$\Delta\%R^\ddagger$
1000	15	0.650	0.310	39.379	43.122	-8.68	-1.95	0.686	0.114	39.372	42.774	-7.95	-2.74
1000	20	0.000	1.000	40.485	41.721	-2.96	**-5.13**	1.000	0.000	40.086	41.463	-3.32	**-5.72**
1000	30	0.702	0.261	40.499	42.190	-4.01	-4.07	0.738	0.094	40.496	42.259	-4.17	-3.91
1000	40	0.072	0.913	44.135	46.443	-4.97	5.61	0.106	0.361	44.124	42.259	4.41	-3.91
1000	60	0.000	1.000	44.135	43.550	1.35	-0.97	0.000	0.414	43.438	43.131	0.71	-1.92
250	60	0.000	1.000	43.887	45.398	-3.33	3.23	0.000	0.414	44.268	45.133	-1.92	2.63
350	60	0.000	1.000	44.001	44.832	-1.85	1.94	0.000	0.414	44.262	45.176	-2.02	2.73
500	60	0.000	1.000	44.127	44.626	-1.12	1.47	0.000	0.413	44.161	45.393	-2.71	3.22
700	60	0.000	1.000	44.124	43.808	0.72	-0.39	0.001	0.413	44.317	44.254	0.14	0.63
1000	60	0.000	1.000	44.288	43.718	1.30	-0.59	0.000	0.414	44.311	46.618	-4.95	6.00
250	15	0.647	0.313	38.823	44.022	-11.81	0.10	0.683	0.115	38.805	43.926	-11.66	-0.12
350	20	0.663	0.298	39.821	42.574	-6.47	-3.19	0.698	0.109	39.792	42.719	-6.85	-2.86
500	30	0.703	0.261	40.508	43.487	-6.85	-1.12	0.738	0.094	40.506	43.424	-6.72	-1.26
700	40	0.072	0.913	44.160	43.975	0.42	-0.01	0.106	0.361	44.066	44.909	-1.88	2.12
1000	60	0.000	1.000	44.289	43.279	2.33	-1.59	0.000	0.414	44.311	46.735	-5.19	6.27

† Surrogate prediction error according to CFD; ‡ percentage of resistance gain relative to parent hull;
* Represents normalized values within the range; * Surrogate prediction; ** CFD validation.

seems not to be helpful to increase the performance of MF surrogate modeling. Finally, there may also be observed the limits of the static sampling strategy and its inherent uncertainties.

The best attempt for KPLS3 and KPLS4 methods (accomplish 5.13% and 5.72% reductions, respectively) use the same combination of fidelity data as 1000 LF and 20 HF, which has the best performance in surrogate modeling in terms of error metrics. The best optimum hull form for (KPLS4) is compared to the original hull in Fig. 12 and the corresponding performance in terms of wave elevations and pressure distribution on the hull surface can be observed in Fig. 13.

The rest of the constructed surrogates, especially in some cases, are pretty far to be regarded as optimum. Therefore, a number of issues can be discussed for the sake of MF strategy. Finally, Fig. 14 shows the correlation of the 60 HF training points with their LF counterparts. According to this figure, the discrepancy between LF and HF simulations is excessive, making the implementation of MF strategies challenging. Another issue that has to be considered is the amount of data used to train the surrogate model according to the dimension of the problem. For such a high-dimensional SBDO problem, dimension reduction strategies should be examined to maintain the advantage of MF implementation, so as to keep the required number of training HF data as small as possible. Nevertheless, KPLS is able to attain significant reductions in total resistance with a static DoE. Finally, it may be noted that increasing the training set size causes, in some cases, decreased surrogate

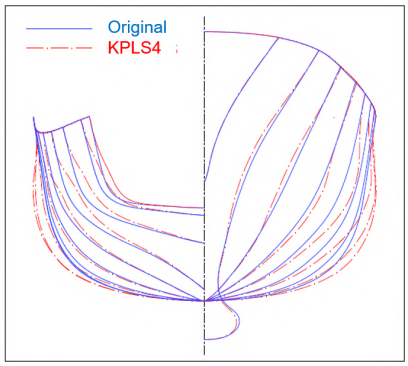

Figure 12: Geometrical comparison of optimal hull forms with parent hull (framework B)

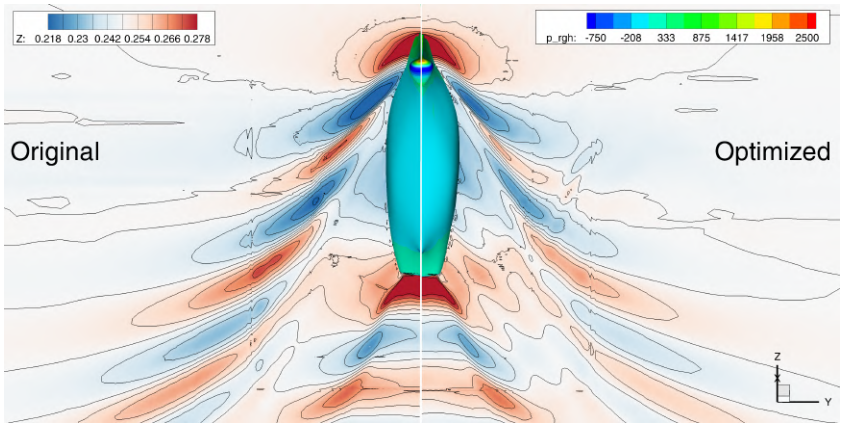

Figure 13: Comparison of original and the optimized wave elevation pattern and pressure field along the hull (framework B)

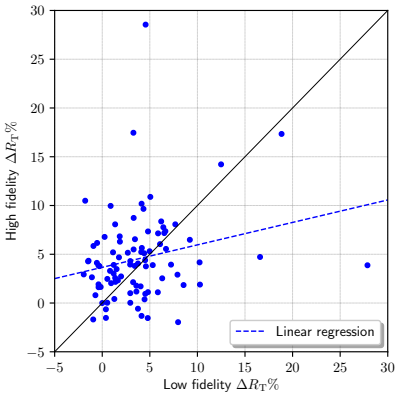

Figure 14: Objective functions correlation for HF and LF numerical solutions (framework B)

accuracy. Alternatively, to enhance the surrogate model strategy, an adaptive sampling strategy may be considered to prevent additional computational costs associated with sampling the unnecessary regions.

4.3 Framework C

RANS (ReFRESCO) is used as both HF and LF solvers. The HF grid consists of approximately 15M cells, whereas the LF grid consists of 1.7M cells, (see Figure 15). The computational cost for the low-fidelity solution takes approximately 22 minutes using 240 cores on 10 nodes where each node has 2 Intel(R) Xeon(R) Gold 6126 CPU @ 2.60 Hz 12 core CPUs. Using the same resources, the high-fidelity computation takes about 165 minutes to complete (note that the computational cost includes the grid generation process). This reflects in a computational cost ratio equal to 0.13. A CCF design of experiments is used for both the initial high- and low-fidelity sampling plans. The rationale behind this choice is that it provides a relatively coarse initial sampling plan, leaving more budget for the adaptive phase of the optimization method. A budget of 10 is given to the optimization procedure.

The KG-AEI method finds has achieved a total resistance reduction of about 1.05%. The reduction of the pressure resistance is 3.72%, while no significant reduction of the frictional resistance is observed. During the initial exploration phase of the multi-fidelity optimization method, the algorithm decides

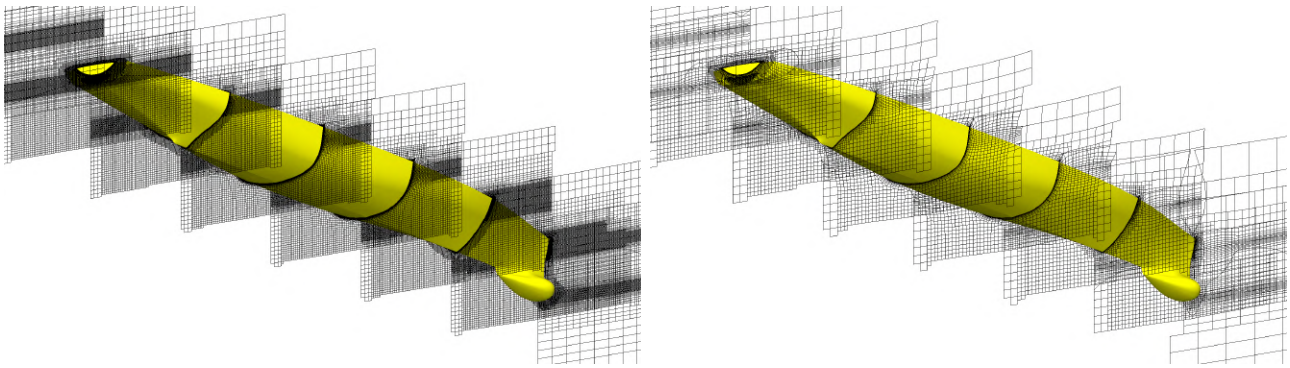

Figure 15: Computational grids for HF (left) and LF (right) solvers (framework C)

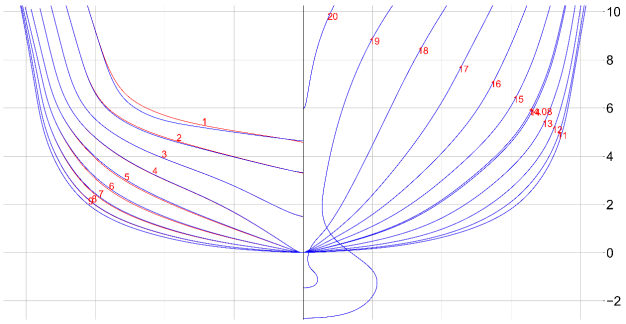

Figure 16: Geometrical comparison of optimal hull forms with parent hull (framework C)

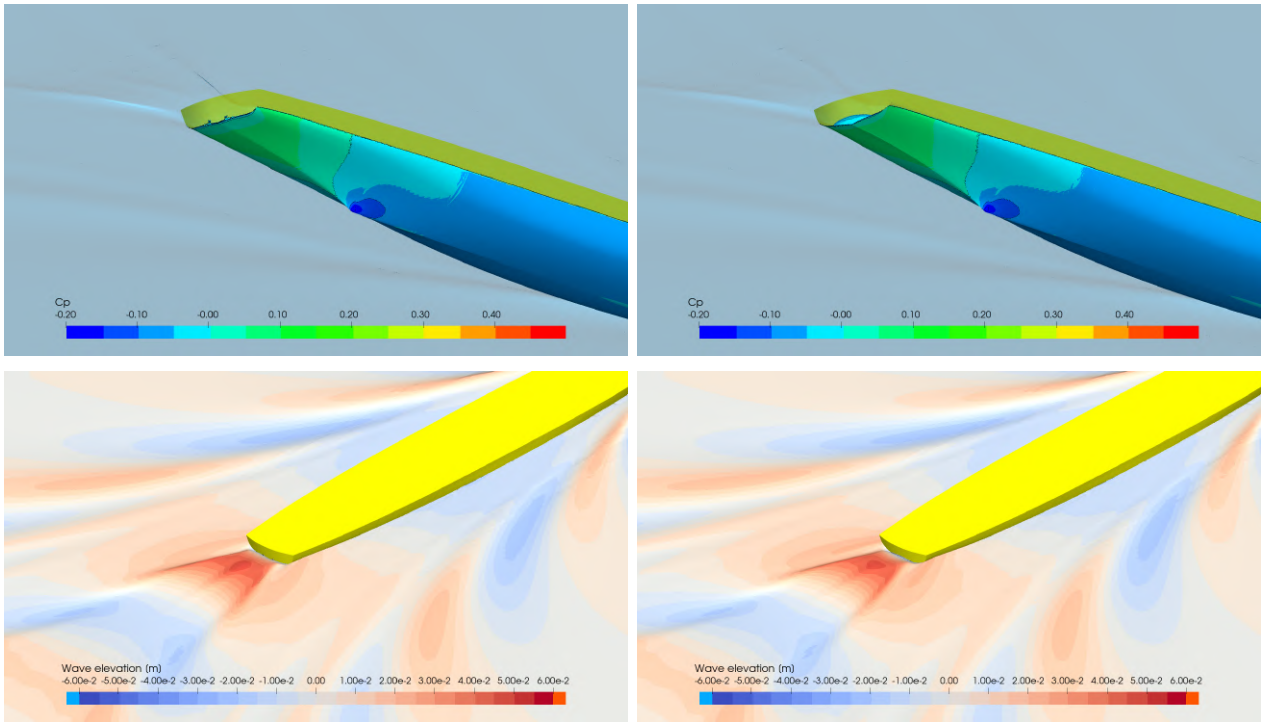

(a) Original hull

(b) Optimized hull

Figure 17: Hull pressure (top) and stern wave system (bottom), before and after the optimization with framework C

to trade 2 HF evaluations for 18 LF evaluations (resulting in a final budget of 10.42). The optimal hull shapes are shown in 16, it is very similar but differs in the amount of V-shape applied to the aft-ship. Finally, 17 shows the pressure coefficient (top) and the stern waves system (bottom) before and after the optimization. It can be seen that the optimized hull has a better pressure recovery than the original hull. This results in reduced pressure resistance and a small increase in the dynamic trim with 0.01 deg, bow down. The stern waves from the optimized hull are slightly less pronounced than the stern waves from the original hull.

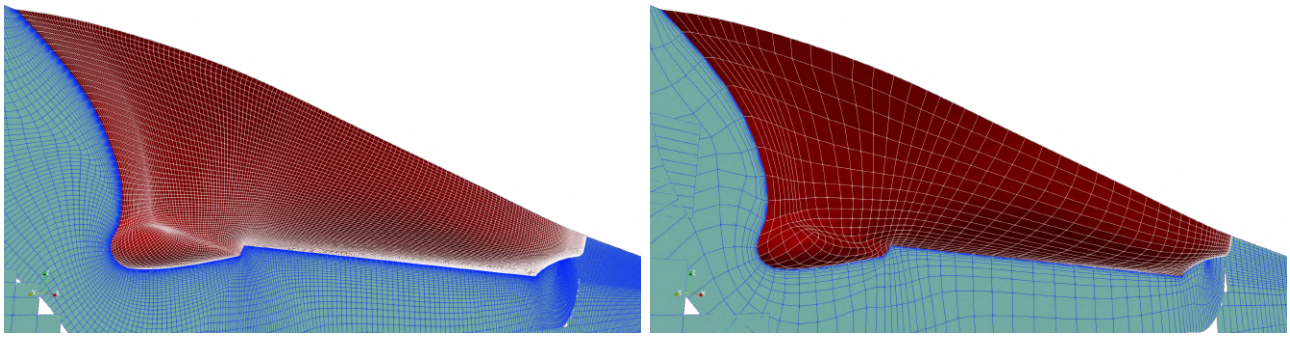

Figure 18: Computational grids for HF (left) and LF (right) solvers (framework D)

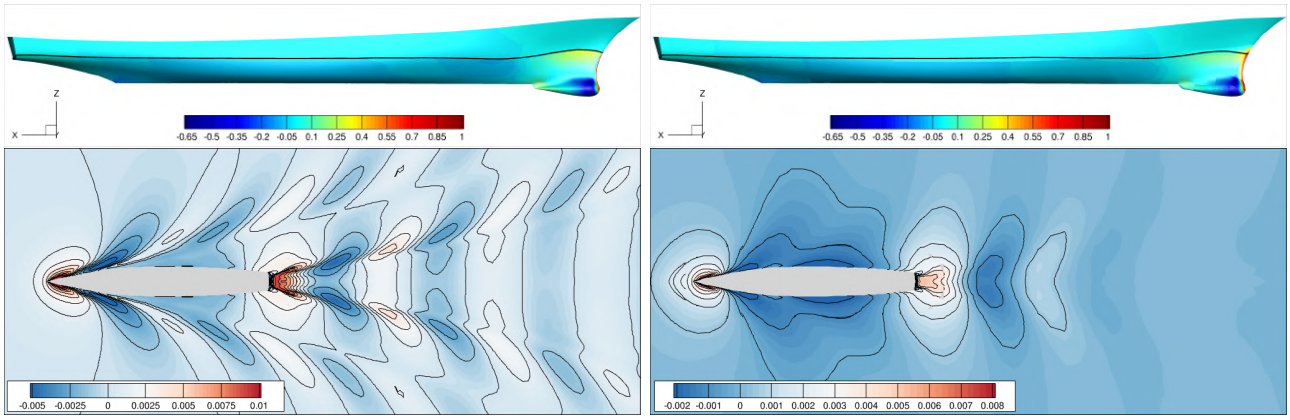

Figure 19: Comparison of HF (left) and LF (right) pressure field along the original hull (top) and wave elevation pattern (framework D)

4.4 Framework D

URANS (χnavis) computations are used to evaluate calm-water performance. Solver multi-grid capability is used for MF purposes. Specifically, two grids composed of 3.6M and 56K grid points (corresponding to the finest and the coarse grid levels of the multi-grid algorithm) are used as high- and low-fidelity levels, respectively shown in Fig. 18 left and right. A comparison of HF and LF pressure fields and wave elevation patterns for the original hull is shown in Fig. 19.

MF surrogate model begins with an initial training set composed of a CCF for the LF level, corresponding to 45 training points, and only 1 HF training point in the domain center. The optimization algorithm is terminated when 45 HF samples are added to the training set. The optimum is achieved by training the SRBF method with 45 HF and 424 LF evaluations, providing 14.4% resistance reduction in calm water at even keel. Comparison with the original pressure distribution along the hull and wave elevation pattern is shown in Fig. 20. The optimized hull provides a significantly reduced wave elevation for both bow and stern diverging Kelvin waves.

4.5 Framework E

It is well known that potential flow codes implementing the boundary element method are quite efficient and reliable in modeling the effect of various geometrical design parameters on the hydrodynamic performance of ships in calm water for the major part of the hull form except for the stern region. In

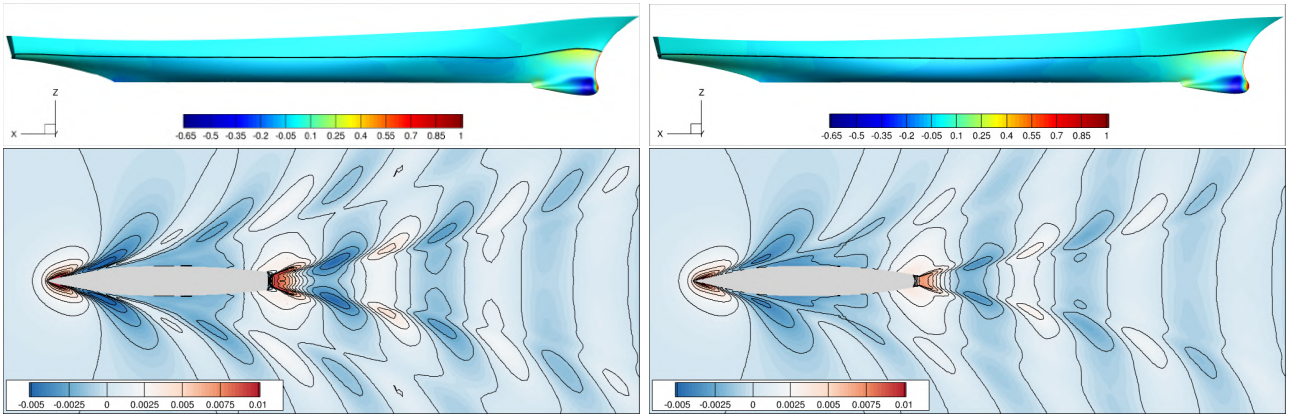

Figure 20: Comparison of (top) pressure field along the hulls and (bottom) wave elevation pattern for the original (left) and optimized vessel (right) for framework D

the latter area, the viscous phenomena dominate and the potential flow modeling is poor. Thus, the potential flow results for the sonar dome and the middle part of the hull form are combined with a surrogate based on an ANN trained by viscous flow results to account for the effect of the stern local design parameters on its hydrodynamic performance.

The mixed-fidelity approach uses a combination of low-fidelity computational solutions (potential code) with ANN predictions of high-fidelity information (viscous runs). ANNs are used to model or detect complex nonlinear relationships within systems without using the physics of the system. Mixed-fidelity optimization is performed in two separate steps; firstly, for the stern region and afterward for the middle and bow region of the vessel. This methodology assumes that the effect of the stern design parameters on the performance of the whole hull is not altered significantly when the bow and the middle design variables are modified. In other words, this assumption is expressed in terms of the (at least partial) independence of the effects of the stern design variables from the rest ones. A limited number of viscous runs is carried out to train an ANN to account for the viscous effects of the vessel's stern region. Specifically, the ANN is trained with only 27 viscous runs as input, which correspond to the 33 combinations of three values per variable (the two selected limiting ones and the value of the parent hull) for the three chosen stern geometrical variables affecting the optimization scheme. Once the ANN is trained sufficiently to constitute a reliable surrogate, the first optimization step consists of the ANN function's minimization, in order to derive the combination of stern parameters that minimize hull viscous resistance, as predicted by the ANN. In the second step, the sonar dome and middle ship geometrical variables are optimized while maintaining the parent form for the stern of the hull in order to minimize wave resistance. Finally, all the geometrical variables, those in the bow and the middle section of the hull, as well as those in the stern region, as tuned by the two optimization cycles are combined in one fair hull.

For the RANS (MaPFlow) simulations, half of the hull was resolved with symmetry conditions applied on the side in order to reduce the computational cost. The high-Reynolds number of full-scale simulations poses a significant challenge since fully resolved viscous simulations are computationally prohibitive. Following a grid-independence study, a grid consisting of approximately 3.5M cells was employed. In the wall region, wall functions were employed. Nevertheless, a structured-like region composed of 25 layers was used around the solid boundary and the hull was resolved using approximately 225k elements. The span of the domain was $8L_{\text{pp}}$ in the streamwise direction, $4L_{\text{pp}}$ in the lateral direction, and $6L_{\text{pp}}$ in the vertical direction. On the ship hull, a no-slip condition was applied, symmetry (zero gradients in the normal direction) conditions were applied on the symmetry plane,

and a freestream condition was imposed on the rest of the domain. Additionally, a damping zone was adopted to avoid reflections from the generated wave system. The average y^+ was 150, with a maximum of 300, consequently, wall functions were adopted. Unfortunately, this was a mandatory compromise cost-wise in order to make full-scale simulations feasible. For all the CFD simulations, a time step of 0.05 s was employed using a second-order implicit scheme which yields a convective CFL of around 4.5. Nevertheless, it was adopted to save computational time since the flows considered here converge to a steady state. It is evident from Figure 21 that both the time step and the grid spacing selected are tuned in order to properly capture the resulting wave system.

(U)RANS calculations were carried out for the 27 hull variants in order to evaluate the effect of stern geometrical variables and create the training set of the ANN, for the validation of potential flow (LF) results and, lastly, for the evaluation of the final hull as emerged from the proposed methodology. The use of limited viscous calculations is an advantage of the proposed methodology but also a challenge in order to create a reliable ANN model. For that matter, training data normalization and selection of a suitable neural network architecture are crucial. In this study, a custom Min/Max feature scaling was employed for the dataset with a 3% reserve. This reserve was used in order to ease the first step of the optimization process, ANN's function minimization, by allowing us to extrapolate values

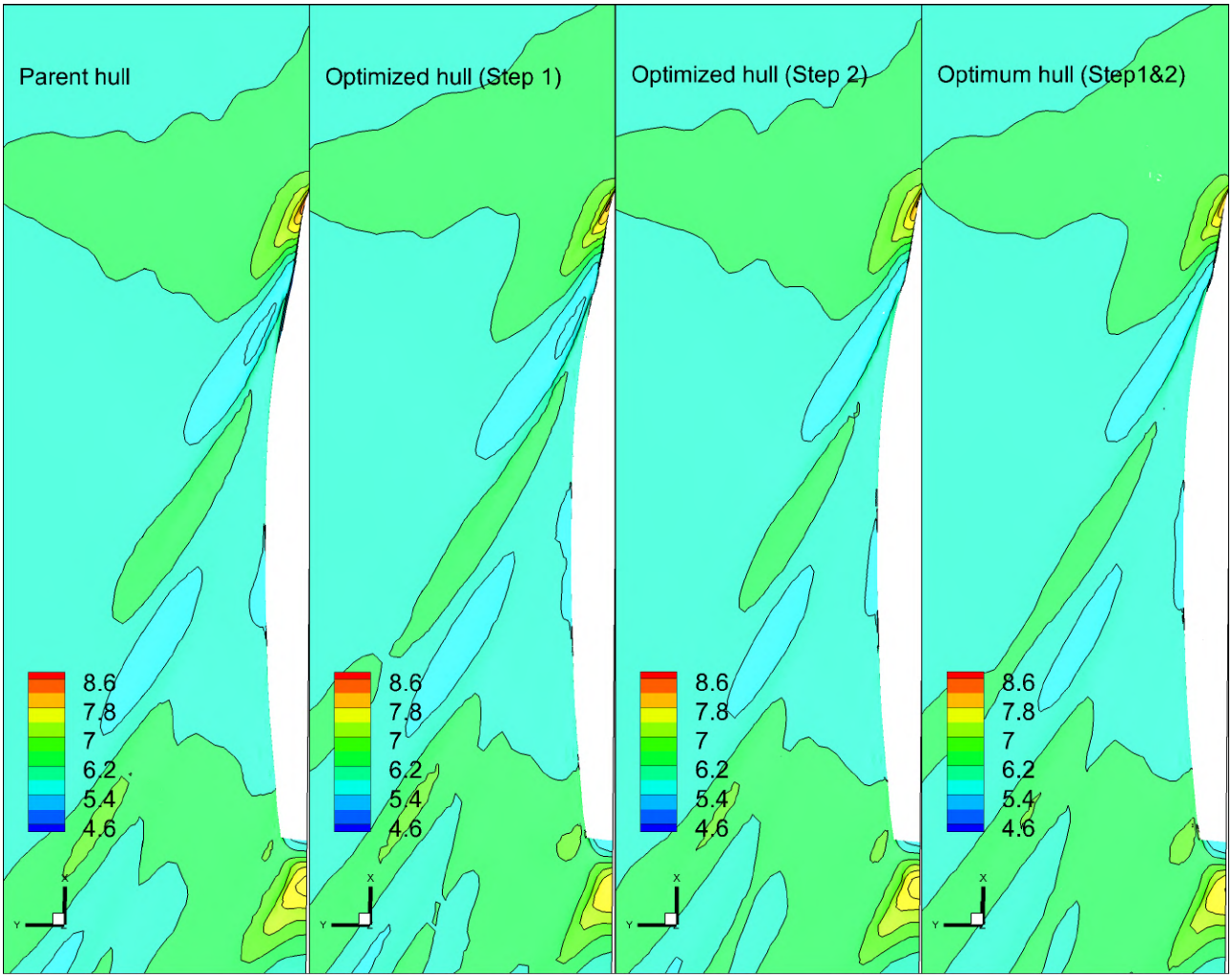

Figure 21: L3 sea benchmark: comparison of free surface elevation for all optimization steps, framework E

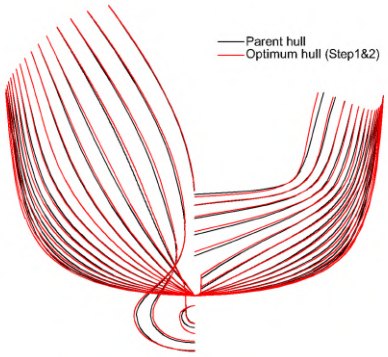

Figure 22: Comparison of original and optimized hull stations (framework E)

beyond observed values representing R_T. For ANN's function minimization NSGA-II algorithm Deb et al. (2002) was executed. No validation set was used due to the small size of the training data. The architecture of the neural network that showed excellent agreement with the input training data was optimized against its mean square error. The scarcity of training data led to employing a small learning rate and momentum, whilst a large number of training epochs (scale of 5×10^5) was needed. Despite a large number of epochs, the training procedure required less than 10 min to complete on an Intel i7 9700K. It is noted that the trade-off between the number of viscous evaluations for the creation of a larger training set and an efficient neural network depends on the hull form, the selected geometrical variables, the magnitude of their variance, and the complexity of vessel shape in the stern region.

In the second step of the optimization procedure, the six design variables at the sonar dome and the middle region of the vessel went through another NSGA-II optimization cycle. This time, hull variants were evaluated via the potential solver SWAN2. It should be noted that the vessel's stern region was

Table 5: Stern shape optimization (framework E - step 1)

Stern Parameters	Optimum	Δ%
Maximum Beam at Station 0 [m]	6.583	-4.86
Wedge Depth [m]	0.177	17.70
Height of Skeg [m]	2.241	14.45
WSA (at speed)	3035	-0.15
R_T [kN]	353	-10.17

Table 6: Bow and middle region optimization (framework E - step 2)

Stern Parameters	Optimum	Δ%
Maximum beam of sonar dome [m]	3.3	3.12
Angle of Entrance [deg]	188.38	-1.01
Maximum Beam at WL [m]	9.76	2.43
Aft longitudinal position of sonar dome's lower profile [m]	126.02	-0.14
Longitudinal position of sonar dome's maximum beam [m]	136.89	0.65
Sonar dome's tip elevation (for the most forward point of sonar dome's length) [m]	-1.68	29.23
WSA (at speed)	3069	1.02
R_W [kN]	81.3	-15.31

kept in parent shape. The free surface (half symmetric plane) was meshed with 5.2k panels, while 1.8k panels were distributed over the hull surface (demi-hull). For the emerged best design, potential flow results showed a 15% reduction of R_W, whereas viscous evaluation of that hull design estimated a 5% reduction of the R_T. The results of both optimization steps are presented in Tables 5 and 6, respectively.

As a final step, the optimum design variables as those that emerged from both optimization steps were combined to derive the overall optimized hull form, presented in Figure 22. Its performance was assessed via viscous calculation and the results showed a reduction of around 11.7% at the R_T.

5. CONCLUSIONS

The paper presented and discussed the resistance optimization of a destroyer-type vessel, namely the DTMB 5415 model, by means of several multi-fidelity approaches. They were presented and discussed, with application to a (global) design optimization problem of the same vessel. Different hull-form parameterization methods were applied, based on free-form deformation, Akima's surface generation, hull blending, and CAD parametric modeling. Furthermore, a dimensionality reduction procedure via parametric model embedding was used to obtain a reduced-dimensionality representation of high-dimensional design spaces, introducing a multi-fidelity approach in the hull-form representation. Physical models and numerical solvers include unsteady Reynolds-averaged Navier-Stokes and potential flow. Different solvers and spatial discretizations were used as different information sources in multi-fidelity optimization. Different multi-fidelity integration approaches were discussed, exploring static and dynamic surrogate models, as well as mixed approaches. As surrogate models, stochastic radial basis functions, Kriging, Kriging with partial least squares, and artificial neural networks were investigated. Multi-fidelity versions of the lower confidence bounding and augmented expected improvement were used for the active learning process (adaptive sampling) of surrogate models. Finally, five computational multi-fidelity frameworks were individually applied, combining different physical models/solvers, hull-form parameterization approaches, and multi-fidelity integration methods.

The outcomes of the work have highlighted how the dimensionality of the optimization problem (i.e., the design space dimensionality) may be a critical issue for the (global) surrogate model training, which is certainly true also and especially if only high-fidelity evaluations are used. In the present context, the proposed multi-fidelity approaches were able to achieve significant objective-function improvements, even if only a few high-fidelity evaluations were used, which is one of the most valuable outcomes of the present collaborative research effort. Specifically, the ratio between the number of high- and low-fidelity evaluations required to solve the global optimization problem was found as low as nearly 1/50. Furthermore, a viable option for improving the training process by overcoming the curse of dimensionality was presented and discussed using a parametric model embedding approach. This allows to reduce the design-space dimensionality before solving the design optimization and/or to train the surrogate model. A prescribed (or arbitrary) level of the original design variability is retained (resolved) by the reduced-dimensionality representation. In the multi-fidelity context, the method provides an additional fidelity level for the representation of hull geometries in the design space. Finally, although the overall agreement between RANS and potential flow solution has shown quite promising results for their combined application in the MF context, the limitation of the potential flow solver, which stems from its inability to properly identify performance losses associated with flow separations that might occur in some regions of the design space, poses a methodological challenge for their use in the MF framework.

The present effort raised the discussion on several research directions for multi-fidelity optimization

environment, such as: (i) the use of non-hierarchical approaches, when high-fidelity physical models with coarse discretizations are used in combination with lower-fidelity models with fine discretizations; (ii) the collaborative solution of the same design problem, where high- and low-fidelity computations are distributed among multiple computational systems, possibly leveraging parallel infill approaches; (iii) the assessment of the relationship between geometric variance and performance variability, along with the development and application of nonlinear approaches to shape reparameterization; finally (iv) the extension of simulation-driven design optimization to incorporate emerging machine learning and artificial intelligence methods, whose effective and efficient integration in the current context needs deeper investigations.

ACKNOWLEDGEMENTS

The present research is conducted in collaboration with "AVT-331 Research Task Group on Goal-driven, multi-fidelity approaches for military vehicle system-level design". CNR-INM's Framework A optimization tools were mostly developed under Office of Naval Research support, through NICOP grant N62909-18-1-2033, administered by Dr. Woei-Min Lin, Dr. Elena McCarthy, and Dr. Salahuddin Ahmed of the Office of Naval Research and Office of Naval Research Global. Framework B studies of ITU is partially supported by TUBITAK via the "Energy Saving Techniques for Energy Efficient Vessels and Emission Reduction towards Green Shipping" project with grant number 218M487.

REFERENCES

Akima, H., 1978. A method of bivariate interpolation and smooth surface fitting for irregularly distributed data points. ACM Transactions on Mathematical Software (TOMS) 4, 148–159.

Bassanini, P., Bulgarelli, U., Campana, E.F., Lalli, F., 1994. The wave resistance problem in a boundary integral formulation. Surveys on Mathematics for Industry 4, 151–194.

Beran, P.S., Bryson, D., Thelen, A.S., Diez, M., Serani, A., 2020. Comparison of multi-fidelity approaches for military vehicle design, in: AIAA AVIATION 2020 FORUM, p. 3158.

Bouhlel, M.A., Bartoli, N., Otsmane, A., Morlier, J., 2016. Improving kriging surrogates of high-dimensional design models by partial least squares dimension reduction. Structural and Multidisciplinary Optimization 53, 935–952.

Broglia, R., Durante, D., 2018. Accurate prediction of complex free surface flow around a high speed craft using a single-phase level set method. Computational Mechanics 62, 421–437.

Byrd, R.H., Lu, P., Nocedal, J., Zhu, C., 1995. A limited memory algorithm for bound constrained optimization. SIAM J. Sci. Comput. 16, 1190–1208.

Dawson, C.W., 1977. A practical computer method for solving ship-wave problems, in: Proceedings of the 2nd International Conference on Numerical Ship Hydrodynamics, Berkeley. pp. 30–38.

Deb, K., Pratap, A., Agarwal, S., Meyarivan, T., 2002. A fast and elitist multiobjective genetic algorithm: Nsga-ii. Evolutionary Computation, IEEE Transactions on 6, 182–197.

Di Mascio, A., Broglia, R., Favini, B., 2001. A Second Order Godunov–Type Scheme for Naval Hydrodynamics. Kluwer Academic/Plenum Publishers, Boston, MA, USA. pp. 253–261.

Di Mascio, A., Broglia, R., Muscari, R., 2007. On the Application of the One–Phase Level Set Method for Naval Hydrodynamic Flows. Computers & Fluids 36, 868–886.

Di Mascio, A., Broglia, R., Muscari, R., 2009. Prediction of hydrodynamic coefficients of ship hulls by high-order Godunov-type methods. Journal of Marine Science and Technology 14, 19–29. doi:10.1007/s00773-008-0021-6.

Grigoropoulos, G., Campana, E.F., Diez, M., Serani, A., Goren, O., Sarioz, K., Danisman, D., Visonneau, M., Queutey, P., Abdel-Maksoud, M., Frederick, S., 2017. Mission-based hull-form and propeller optimization of a transom stern destroyer for best performance in the sea environment, in: Proceedings of the VII International Congress on Computational Methods in Marine Engineering-MARINE.

Huang, D., Allen, T.T., Notz, W.I., Miller, R.A., 2006. Sequential kriging optimization using multiple-fidelity evaluations. Structural and Multidisciplinary Optimization 32, 369–382.

Huang, J., Carrica, P.M., Stern, F., 2008. Semi-coupled air/water immersed boundary approach for curvilinear dynamic overset grids with application to ship hydrodynamics. International Journal for Numerical Methods in Fluids 58, 591–624.

Langtry, R.B., Menter, F.R., 2009. Correlation-based transition modeling for unstructured parallelized computational fluid dynamics codes. AIAA journal 47, 2894–2906.

Maisonneuve, J.J., 1989. Resolution du probleme de la resistance de vagues des navire par une metode de singularities de Rankine. Ph.D. thesis. University of Nantes.

Menter, F.R., 1994. Two-equation eddy-viscosity turbulence models for engineering applications. AIAA journal 32, 1598–1605.

Olivieri, A., Pistani, F., Avanzini, A., Stern, F., Penna, R., 2001. Towing tank, sinkage and trim, boundary layer, wake, and free surface flow around a naval combatant INSEAN 2340 model. Technical Report. DTIC.

Pellegrini, R., Wackers, J., Broglia, R., Serani, A., Visonneau, M., Diez, M., 2022. A multi-fidelity active learning method for global design optimization problems with noisy evaluations. Engineering with Computers , 1–24.

Posa, A., Broglia, 2019. An immersed boundary method coupled with a dynamic overlapping-grids strategy. Computers & Fluids 191, 104250. doi:doi.org/10.1016/j.compfluid.2019.104250.

Sadat-Hosseini, H., Kim, D.H., Toxopeus, S., Diez, M., Stern, F., 2015. Cfd and potential flow simulations of fully appended free running 5415m in irregular waves, in: World Maritime Technology Conference, Providence, RI, Nov, pp. 3–7.

Schlichting, H., Gersten, K., 2000. Boundary-Layer Theory. Springer-Verlag, Berlin.

Scholcz, T., Klinkenberg, J., 2022. Efficient hull-form optimisation using multi-fidelity techniques, in: AVT-354 Research Workshop on Multi-fidelity methods for military vehicle design, Varna, Bulgaria.

Sederberg, T.W., Parry, S.R., 1986. Free-form deformation of solid geometric models, in: Proceedings of the 13th annual conference on Computer graphics and interactive techniques, pp. 151–160.

Serani, A., Diez, M., 2023. Parametric model embedding. Computer Methods in Applied Mechanics and Engineering 404, 115776.

Serani, A., Diez, M., Campana, E.F., Fasano, G., Peri, D., Iemma, U., 2015. Globally convergent hybridization of particle swarm optimization using line search-based derivative-free techniques, in: Yang, X.S. (Ed.), Recent Advances in Swarm Intelligence and Evolutionary Computation. Springer International Publishing. volume 585 of *Studies in Computational Intelligence*, pp. 25–47.

Serani, A., Diez, M., van Walree, F., Stern, F., 2021. URANS analysis of a free-running destroyer sailing in irregular stern-quartering waves at sea state 7. Ocean Engineering 237, 109600.

Serani, A., Fasano, G., Liuzzi, G., Lucidi, S., Iemma, U., Campana, E.F., Stern, F., Diez, M., 2016a. Ship hydrodynamic optimization by local hybridization of deterministic derivative-free global algorithms. Applied Ocean Research 59, 115 – 128.

Serani, A., Ficini, S., Broglia, R., Diez, M., Grigoropoulos, G., Bakirtzogou, C., Goren, O., Danisman, D., Pehlivan, H.S., Yildiz, S., Nikbay, M., Scholcz, T., Klinkenberg, J., 2022a. Resistance and seakeeping optimization of a naval destroyer by multi-fidelity methods, in: AVT-354 Research Workshop on Multi-fidelity methods for military vehicle design, Varna, Bulgaria.

Serani, A., Leotardi, C., Iemma, U., Campana, E.F., Fasano, G., Diez, M., 2016b. Parameter selection in synchronous and asynchronous deterministic particle swarm optimization for ship hydrodynamics problems. Applied Soft Computing 49, 313–334.

Serani, A., Pellegrini, R., Broglia, R., Wackers, J., Visonneau, M., Diez, M., 2019. An adaptive N-fidelity metamodel for design and operational-uncertainty space exploration of complex industrial problems, in: VIII International Conference on Computational Methods in Marine Engineering MARINE.

Serani, A., Stern, F., Campana, E.F., Diez, M., 2022b. Hull-form stochastic optimization via computational-cost reduction methods. Engineering with Computers 38, 2245–2269.

Spalart, P., Allmaras, S., 1992. A one-equation turbulence model for aerodynamic flows, in: 30th aerospace sciences meeting and exhibit, p. 439.

Storn, R., Price, K., 1997. Differential evolution–a simple and efficient heuristic for global optimization over continuous spaces. Journal of global optimization 11, 341–359.

Venkatakrishnan, V., 1993. On the accuracy of limiters and convergence to steady state solutions, in: 31st Aerospace Sciences Meeting, p. 880.

Wackers, J., Pellegrini, R., Diez, M., Serani, A., Visonneau, M., 2022. Improving active learning in multi-fidelity hydrodynamic optimization, in: 34th Symposium on Naval Hydrodynamics.

Yue, J.s., Wu, S.p., 2018. An improvement to the kunz preconditioner and numerical investigation of hydrofoil interactions in tandem. International Journal of Computational Fluid Dynamics 32, 167–185.